

Article

An Improved PLL-Based Speed Estimation Method for Induction Motors through Harmonic Separation

Jie Yu *, Youjun Zhang and Xiaoqin Zheng

College of Electrical Engineering, Qingdao University, Qingdao 266071, China

* Correspondence: yujie_ee@qdu.edu.cn

Abstract: The real-time speed estimation of induction motors (IMs) is important for the motors' state monitoring and control. The utilization of rotor slot harmonics (RSHs) due to the inherent cogging effect is regarded as a promising way to realize the speed estimation of IMs. The key to the RSH-based speed estimation method is how to accurately and quickly identify the frequency of an RSH signal. However, as the RSH signal always consists of two side-frequency components that are adjacent to each other, it is actually improper to directly use the conventional phase-locked loop (PLL) method designed for single-frequency tracking. Furthermore, the form of the two side components in the frequency domain also leads to a significant amplitude fluctuation in the time-domain waveform of RSHs, thus resulting in the obvious frequency tracking errors of the conventional PLL method. In this paper, we proposed an improved PLL through harmonic separation to further improve the performance of the RSH-based speed estimation method of multiphase IMs, so that the dynamic tracking errors of PLL due to the reasons mentioned above can be significantly reduced. Simulations and experiments in a wide speed range were also performed, with their results presented as verifications of the proposed method.

Keywords: induction motor; speed estimation; phase-locked loop; motor harmonics



Citation: Yu, J.; Zhang, Y.; Zheng, X. An Improved PLL-Based Speed Estimation Method for Induction Motors through Harmonic Separation. *Energies* **2022**, *15*, 6626. <https://doi.org/10.3390/en15186626>

Academic Editor: Anibal De Almeida

Received: 5 August 2022

Accepted: 5 September 2022

Published: 10 September 2022

Publisher's Note: MDPI stays neutral with regard to jurisdictional claims in published maps and institutional affiliations.



Copyright: © 2022 by the authors. Licensee MDPI, Basel, Switzerland. This article is an open access article distributed under the terms and conditions of the Creative Commons Attribution (CC BY) license (<https://creativecommons.org/licenses/by/4.0/>).

1. Introduction

The real-time and accurate speed measurement of induction motors is important to monitor the operation condition of the motors or achieve high performance in speed control. Conventional speed sensors, such as rotational transformers or photoelectrical encoders, are generally installed coaxially on the motor to accomplish the measurement. However, these sensors are generally vulnerable to water immersion, rotor eccentricity, vibrations, and shocks [1], so the sensors may face the risk of failure under harsh industrial applications, such as ship propulsion or industrial production. In this case, the online speed estimation of induction motors is essential, as the speed sensor fault can be inherently avoided, contributing to a reduction in system cost and an increase in system reliability.

Various methods have been proposed to realize the speed estimation of induction motors, within which the model-based method and high-frequency signal injection method are commonly used in industry for the condition monitoring or control of induction motors. As an induction motor is a complex electromechanical system with features such as multiple variables, time variations, strong coupling, and uncertainty, its commonly used mathematical model is established under several assumptions and simplifications. Therefore, model-based speed estimation methods often suffer disturbances and uncertainties from unmodeled system dynamics as well as parameter variations. Online identification algorithms for complicated parameters are actually essential to maintain the accuracy of this kind of speed estimation method. Comparatively, high-frequency signal injection methods are more robust to model errors, but special structural designs or external high-frequency signal injections are often needed to construct magnetic saliency.

The well-known cogging effect, which is due to the slotting of the stator and the rotor, introduces an inherent magnetic saliency and results in slot harmonics in both the phase

current and the induced electromotive force. As the slot harmonics due to rotor slotting contain information about motor speed, it is possible to realize a real-time speed estimation by analyzing the frequency properties of rotor slot harmonics [2], with no special design for motor structure or additional high-frequency signal injection.

Among the available frequency analysis methods that are suitable for rotor slot harmonics (RSHs), such as fast Fourier transform (FFT), wavelet analysis (WA), phase-locked loop (PLL) [3], etc., the PLL is believed to be effective in the real-time identification of the frequency of input signal and has a quick response time that is valuable for the dynamic performance of speed estimation [4]. Shen [5] used PLL to track the third-order EMF harmonics and achieved an ultrahigh-speed (120 kr/min) drive of BLDC. Song [6] proposed a fractional-N phase-locked loop (FN-PLL) and a synchronous frequency-extract filter (SFF) to detect the commutation position of a high-speed PMSM. Orfanoudakis [7] investigated the application of second-order generalized integrator (SOGI) PLL under the asymmetry of the currents supplied to the motor. PLL has also been utilized in the high-frequency-injection-based sensorless control of PMSMs. In fact, there is always a compromise between the stability and response time of PLLs [8,9], especially under disturbances [10]. Filipović [11] studied the performance of PLL-based repetitive controls under sudden frequency changes. Yang [12] evaluated the effect of unbalance loads on the PLL-based power control of multilevel converters. Novak [13] introduced an adaptive quadrature PLL in the sensorless control of high-speed PMSMs for improved dynamics.

The key to the RSH-based speed estimation method is to accurately and quickly identify the frequency of an RSH signal. However, as the RSH signal always consists of two side-frequency components that are adjacent to each other [14,15], it is actually improper to utilize a conventional phase-locked loop (PLL) method to effectively identify the frequency of the RSH signal. Furthermore, the form of the two side components in the frequency domain also leads to a significant amplitude fluctuation in the time-domain waveform of RSH, thus resulting in the obvious frequency tracking errors of the conventional PLL method. In this paper, we proposed an improved PLL through harmonic separation to further improve the performance of the RSH-based speed estimation method of multiphase IMs. The time-domain properties of RSHs were firstly analyzed, and a frequency separation algorithm was embedded to preprocess the RSHs so that their amplitude fluctuation would be eliminated. Then, the proposed real-time speed estimation method through the RSH frequency identification was defined and implemented. Finally, simulations and experimental verifications were carried out on a nine-phase induction motor platform under different speed and load conditions.

2. The Time and Frequency Properties of Rotor Slot Harmonics in IMs

2.1. The Analytical Model of RSHs for Multiphase IMs

The rotor slot harmonics are generally regarded as undesired disturbances that not only affect the motor efficiency but also generate cogging ripples. Although the approaches of magnetic slot wedge or slot skewness are generally applied to weaken the effect of RSHs, these kinds of harmonics are actually inherent in the motor's voltage and current, as well as the air-gap magnetic field, if only the rotor is slotted.

To analyze the time and frequency properties of RSHs in IMs, the magnetic potential and permeability methods were used here. Among the different-order RSHs, we took the first or primary rotor slot harmonics (PSHs) as an example; the time-domain expression of PSH consists of two parts: The first one is generated by the fundamental magnetic potential of the motor, along with the magnetic conductivity due to slot cogging effect, and the other one is caused by the interaction between the RSH-induced magnetic potential and the DC component of the air-gap magnetic conductivity. By combining the two parts, the PSH can

be modeled as the combination of two side-frequency components, $B_{t1-}(\theta, t)$ and $B_{t1+}(\theta, t)$, as shown in Equation (1) [16].

$$\begin{aligned} B_{t1}(\theta, t) &= B_{t1-}(\theta, t) + B_{t1+}(\theta, t) \\ &= (F_{r(Z_2/p-1)}\Lambda_0 + \frac{1}{2}F_0\Lambda_r) \cos\left[(Z_2 - p)\theta - \left(\frac{Z_2}{p}(1 - s_m) - 1\right)\omega_1 t\right] \\ &\quad + (F_{r(Z_2/p+1)}\Lambda_0 + \frac{1}{2}F_0\Lambda_r) \cos\left[(Z_2 + p)\theta - \left(\frac{Z_2}{p}(1 - s_m) + 1\right)\omega_1 t\right] \end{aligned} \quad (1)$$

where $F_{r(Z_2/p-1)}$ and $F_{r(Z_2/p+1)}$ are the amplitudes of rotor cogging MMFs, Λ_0 is the DC component of the air-gap magnetic conductivity, Λ_r is the amplitude of sinusoidal air-gap permeance due to a rotor cogging effect, Z_2 is the rotor slot number, s_m is the slip ratio, p is the motor's pole pair number, θ is the mechanical rotor's position, and ω_1 is the synchronous angular speed of the fundamental component.

It can be seen from Equation (1) that the PSH consists of two side-frequency components that are adjacent to each other with a distance of $2f_1$. The frequencies of the two side components are, respectively, f_{t1-} and f_{t1+} ,

$$f_{t1-} = \left(\frac{Z_2}{p}(1 - s) - 1\right)f_1 = \left(\frac{Z_2 n}{60f_1} - 1\right)f_1 \quad (2)$$

$$f_{t1+} = \left(\frac{Z_2}{p}(1 - s) + 1\right)f_1 = \left(\frac{Z_2 n}{60f_1} + 1\right)f_1 \quad (3)$$

in which f_1 is the frequency of the fundamental magnetic field, and n is the motor's speed in r/min.

Then, by combining Equations (2) and (3), the motor's speed can be obtained as

$$n = \frac{15p}{Z_2}(f_{t1-} + f_{t1+}) \quad (4)$$

Despite the PSH in the air-gap flux field, the f_{t1-} and f_{t1+} components are also induced in the stator voltage and current of the induction motor, which can be measured and identified through PLLs. Then, the key to the implementation of the online speed estimation is to identify the frequency of f_{t1-} and f_{t1+} components in real time. However, it is actually improper to utilize a conventional PLL to track the frequency of PSH, which consists of two side-frequency components rather than an ideal single one.

2.2. The Basic Principle of SOGI-PLL

The phase-locked loop has been widely utilized in motor control, the main purpose of which is to synchronize an output oscillator signal with a reference signal. A typical phase-locked loop consists of a phase detector, a loop filter, and a voltage-controlled oscillator (VCO). Here, we used the well-known second-order generalized integrator (SOGI) PLL [17], as shown in Figure 1, in which the orthogonal components u_α and u_β can be generated from the input voltage signal u in a variety of different ways such as transport delay, Hilbert transform, etc. A widely discussed method is to use a second-order integrator, as shown in Figure 2, which is essentially a notch filter that can selectively tune the orthogonal signal generator to reject other frequencies except the referenced frequency. In the SOGI-PLL, k_p and k_i are the proportional and integral parameters of the loop filter, k_o is the gain coefficient of VCO, and ω_o and ω_{out} are separately the initial and output angular frequency of PLL.

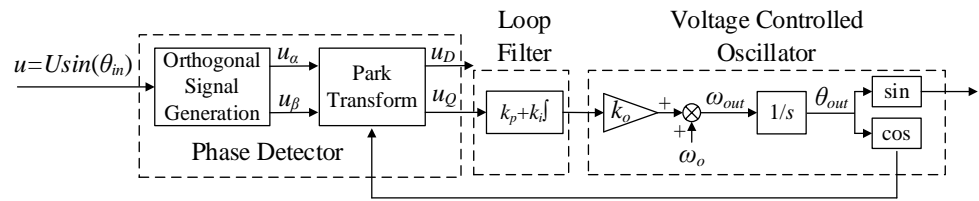


Figure 1. The overall structure of SOGI-PLL.

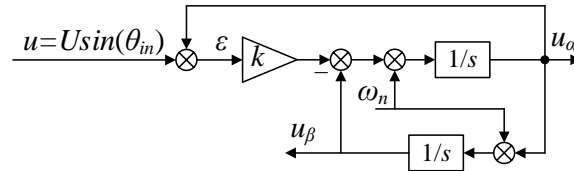


Figure 2. The orthogonal signal generation through SOGI-PLL.

The second-order generalized integrator closed-loop transfer function can be expressed as [18]

$$H_d(s) = \frac{u_\alpha}{u}(s) = \frac{k\omega_n s}{s^2 + k\omega_n s + \omega_n^2} \tag{5}$$

$$H_q(s) = \frac{u_\beta}{u}(s) = \frac{k\omega_n^2}{s^2 + k\omega_n s + \omega_n^2} \tag{6}$$

where $H_d(s)$ is the transfer function from the PLL input u to the output u_α , $H_q(s)$ is the transfer function from the PLL input u to the output u_β , and $s = j\omega$. $k > 1$ is the gain of the orthogonal signal generation block. ω_n is the frequency of the RSH component in radians.

As the frequencies of RSHs keep changing during motor operation, the orthogonal signal generator must be tuned online accordingly. Here, the trapezoidal approximation [19] is used to obtain the discrete transfer function as follows:

$$H_d(z) = \frac{b_0 + b_2 z^{-2}}{1 - a_1 z^{-1} - a_2 z^{-2}} = \frac{\left(\frac{x}{x+y+4}\right) + \left(\frac{-x}{x+y+4}\right)z^{-2}}{1 - \left(\frac{2(4-y)}{x+y+4}\right)z^{-1} - \left(\frac{x-y-4}{x+y+4}\right)z^{-2}} \tag{7}$$

$$H_q(z) = \frac{qb_0 + qb_1 z^{-1} + qb_2 z^{-2}}{1 - a_1 z^{-1} - a_2 z^{-2}} = \frac{\left(\frac{k \cdot y}{x+y+4}\right) + 2\left(\frac{k \cdot y}{x+y+4}\right)z^{-1} + \left(\frac{k \cdot y}{x+y+4}\right)z^{-2}}{1 - \left(\frac{2(4-y)}{x+y+4}\right)z^{-1} - \left(\frac{x-y-4}{x+y+4}\right)z^{-2}} \tag{8}$$

in which the coefficients x and y are separately expressed as

$$x = 2k\omega_n T_s, \quad y = (\omega_n T_s)^2 \tag{9}$$

where T_s is the sampling period.

Once the orthogonal signal is generated, the Q and D components on the rotating reference frame can be obtained through the park transform, while the Q component is then fed to the loop filter, which controls the VCO of the PLL. Therefore, the PLL is a closed-loop system with a control mechanism to reduce any phase error, and its lock can be achieved when the phase difference between the two signals is zero. The coefficient of the PI loop filter k_p and k_i , as shown in Figure 1, can be adjusted as follows:

$$\begin{aligned} \omega_{lf} &= \frac{1}{T_s} \log\left(\frac{1}{\delta\sqrt{1-\xi^2}}\right) \\ k_p &= 2\xi\omega_{lf} \\ k_i &= \frac{k_p\omega_{lf}}{2\xi} \end{aligned} \tag{10}$$

where ω_{lf} is the nominal frequency of the loop filter in radians, t_s is the build-up time, ζ is the damping ratio, and δ is the width of the error band. In this work, these parameters were, respectively, set as $t_s = 50$ ms, $\zeta = 0.7$, and $\delta = 0.01$.

2.3. The Dynamic Tracking Error of PLL Due to the Amplitude Fluctuation of Input Signal

For an input signal with steady frequency and amplitude, a PLL quickly converges and accurately tracks its frequency. However, when the amplitude or frequency of the input signal fluctuates, the “locked” state of the PLL is aborted and transferred into convergence transients, which of course affects the accuracy and dynamic performance of the RSH-based speed estimation.

As an example, for a well-tuned SOGI-PLL, we set a 100 Hz input signal with an initial amplitude of 1 V but suddenly changed it to 0.2 V, and its frequency tracking result is shown in Figure 3. It is clear that the sudden amplitude change in the input signal caused significant frequency tracking errors.

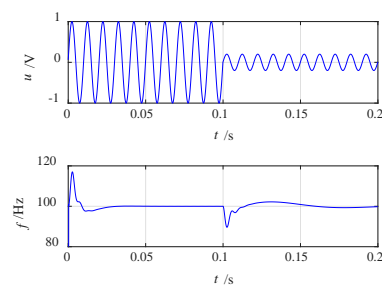


Figure 3. The frequency tracking results of SOGI-PLL when the amplitude of input suddenly changes.

Furthermore, for the primary rotor slot harmonic signal, the synthesis of f_{t1-} and f_{t1} components results in a variation in the time-domain amplitude or modulation of PSH and causes errors affecting the dynamic performance of the PLL. This is illustrated in Figure 4, in which a 105 Hz signal was added to the original 100 Hz signal at 0.4 s, with the signal amplitude of each component kept steady. It can be seen that the synthesized signal was of periodic fluctuated amplitude, which led to significant frequency tracking errors.

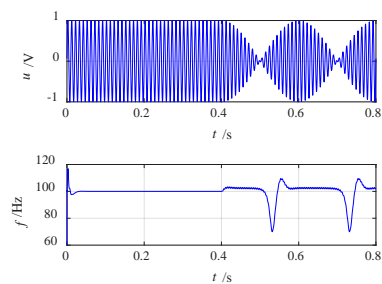


Figure 4. The frequency tracking results of SOGI-PLL for the simulated RSH signal.

3. Harmonic Separation Speed Estimation Method for Multiphase IMs

In order to improve the frequency tracking accuracy of PLLs, a novel frequency separation was proposed in this study to preprocess the PSH signal, so that the f_{t1-} and f_{t1+} components can be adaptively distributed into two independent signals. In this way, the amplitude modulation characteristics are eliminated, and the SOGI-PLL can be utilized to track the frequency of f_{t1-} and f_{t1+} in real time, with satisfying accuracy and dynamic response time.

According to Equations (2) and (3), the f_{t1-} and f_{t1+} components can be extracted by directly using a passband filter with the central pass frequency of f_{t1-} and f_{t1+} . Meanwhile, there is always a frequency separation of $2f_1$ between the two components, which limits the passband of the filters. While the slip ratio s_m is unknown, its value is actually close

to 0 in most working conditions and can be omitted in the following harmonic separation. Therefore, the central frequencies of the harmonic separation filters are designed as

$$f_{hd_t1n} = \left(\frac{Z_2}{p} - 1\right)f_1 \tag{11}$$

$$f_{hd_t1p} = \left(\frac{Z_2}{p} + 1\right)f_1 \tag{12}$$

and the passband of the harmonic separation filters should be lower than $2f_1$, so as to avoid the aliasing error between the f_{t1-} and f_{t1+} components. As f_1 decreases along with the speed, a too-narrow passband appears in the low-speed range. In this case, there is a tradeoff between the high order for filter design and the complete separation of PSHs. In addition, the embedded frequency separation filters also introduce time delay into the speed estimation, which is illustrated in Figure 5, in which i_{t1} the PSH signal in the phase current signal measured by current sensors, and i_{t1-} and i_{t1+} are, respectively, the f_{t1-} and f_{t1+} components separated by the frequency separation filters mentioned above. As Figure 6 shows, the amplitude i_{t1} keeps fluctuating and approaches zero periodically, but the amplitude of i_{t1-} and i_{t1+} are almost steady after the frequency separation processing. This benefits the following frequency identification through SOGI-PLL and results in more accurate speed estimation. However, the implementation of frequency separation filters, through either analog or digital ways, adds time or phase delay to the signal processing of PSH. As an example, a time delay of about 0.02 s is caused by the bandpass Butterworth IIR filter with the order of 4.

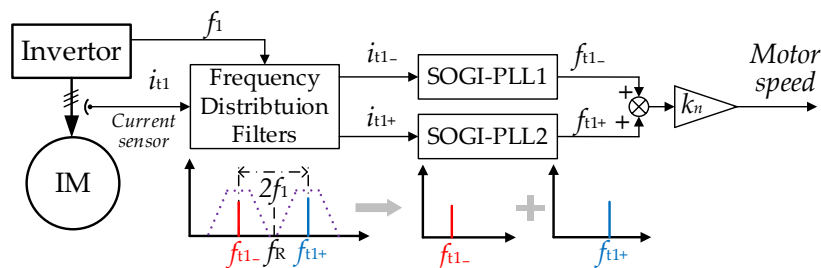


Figure 5. The diagram of the PLL-based speed estimation method for IMs based on harmonic separation.

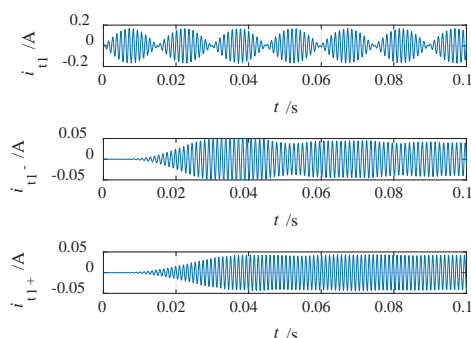


Figure 6. The harmonic separation results of the PSH signal ($n = 973$ r/min, $s = 0.026$).

4. Simulation and Experimental Results

4.1. Experiment Platform Setup

A nine-phase IM platform was established in this study to verify the proposed speed estimation method. The multiphase induction motors are fit for ship electric propulsion and other electrical transportation applications. Its fault-tolerant capability and reduced bus voltage level are the main merits of this method when compared with the usual three-phase ones. As shown in Figure 7, the platform consisted of a nine-phase squirrel-cage induction

motor, a multiphase inverter, a coaxially connected DC generator, and a resistance load box. A rotatory transformer was installed with an accuracy of no less than 0.1 r/min.

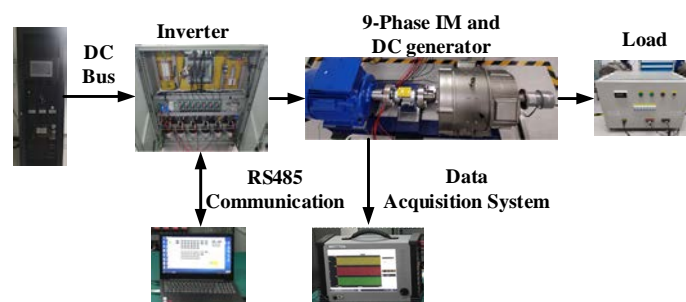


Figure 7. The nine-phase induction motor platform.

As the RSH is an inherent property of each phase current, it is convenient to use one single-phase current sensor to obtain the RSH signal for an induction motor with three or more phases. Comparatively, the conventional model-based method needs more sensors and computation burden, especially for multiphase induction motors. The PSH signal was obtained from the stator current, which was measured through a LEM LA-25P current sensor. The proposed speed estimation method was carried out through the TMS320F28335 DSP. Differential signal measurement and a sigma-delta ADC sample were utilized to improve the SNR. The main parameters of the platform are listed in Table 1.

Table 1. Main parameters of nine-phase induction motor platform.

Symbol	Parameter	Value
P_N	Rated motor power	8 kW
m	Phase number	9
f_N	Rated power supply frequency	50 Hz
p	Pole pairs	2
n_N	Rated speed	1477 r/min
I_N	Rated phase current	12.87 A
Z_2	Rotor slot number	54

4.2. Simulated Speed Estimation Results under Different Speed and Load Conditions

According to the parameters presented in Table 1, the proposed PLL-based position estimation method through harmonic distribution was firstly verified through simulations in MATLAB, in which a PSH signal was generated in reference to Equations (1) and (2). As the key to the realization of the RSH-based speed estimation method is to accurately identify the frequency of the RSH signal, the effectiveness of the proposed method was directly compared with the conventional PLL method. For the conventional PLL method, the PSH signal was directly processed through a SOGI-PLL. As can be seen from Figures 8–13, the proposed method through harmonic separation achieved much better estimation accuracy than the conventional PLL method, within a wide speed range from 200 r/min to 1500 r/min. In these figures, the blue line represents the actual value, and the red line represents the estimated value. However, the harmonic separation process indeed introduced unexpected time delay and transients at the beginning of the estimation, but then the estimated speed quickly converged to the actual value, and the convergence was maintained later.

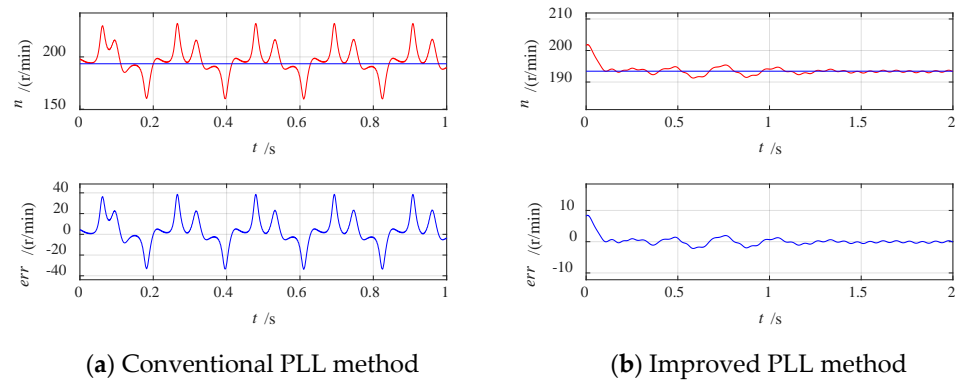


Figure 8. The simulated speed estimation results ($n = 193$ r/min, $s = 0.033$, the blue line: the actual value, the red line: the estimated value, same for Figures 8–13).

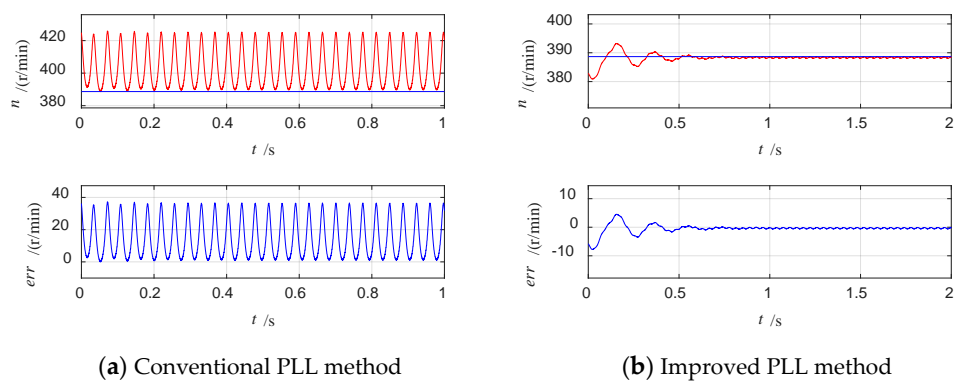


Figure 9. The simulated speed estimation results ($n = 389$ r/min, $s = 0.028$).

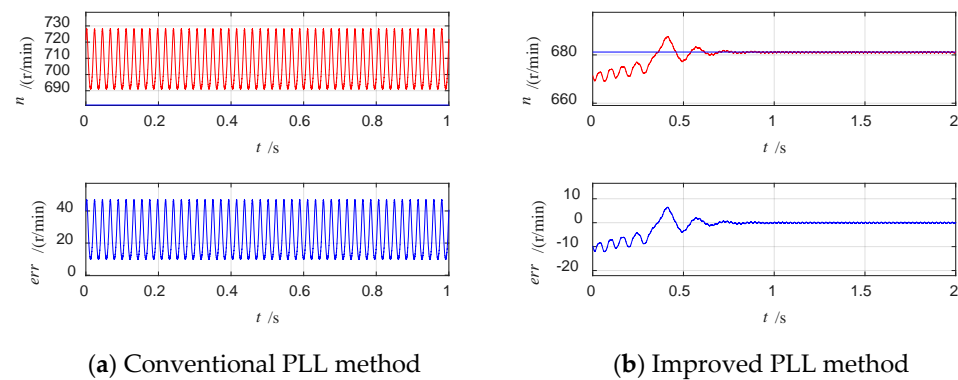


Figure 10. The simulated speed estimation results ($n = 681$ r/min, $s = 0.027$).

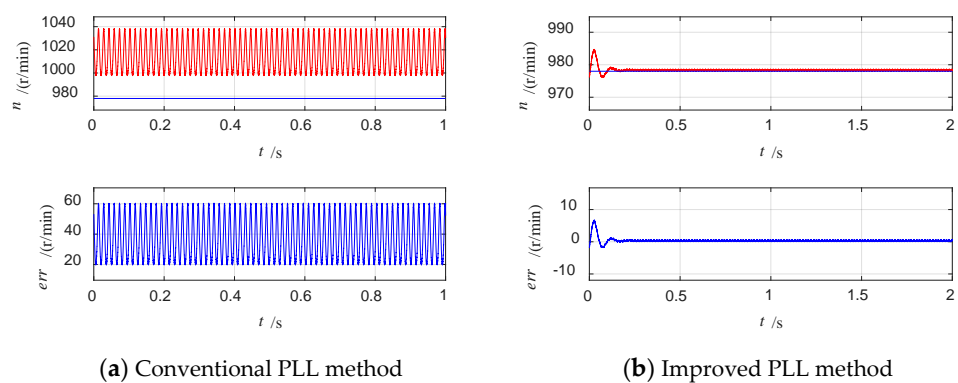


Figure 11. The simulated speed estimation results ($n = 978$ r/min, $s = 0.023$).

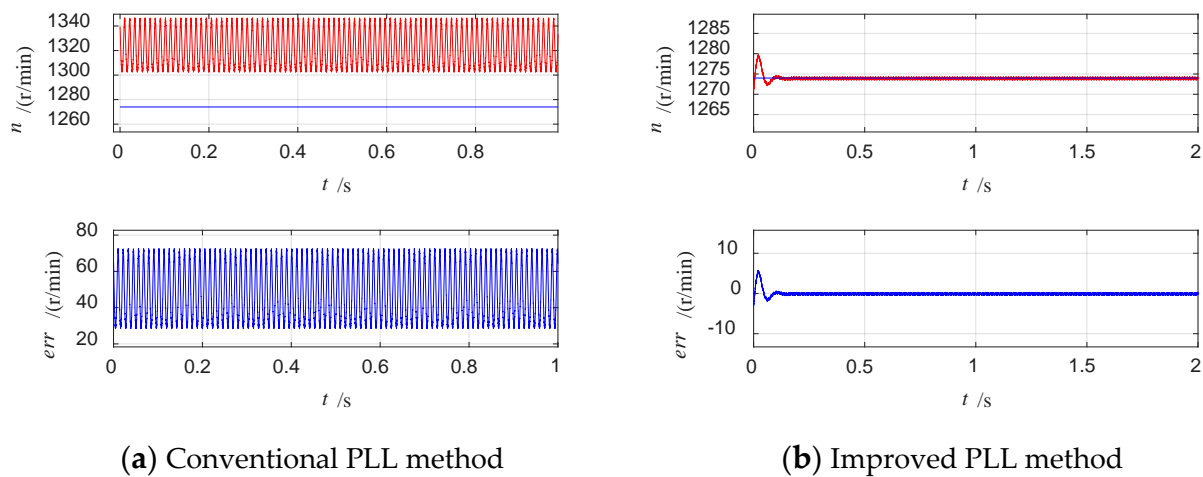


Figure 12. The simulated speed estimation results ($n = 1266$ r/min, $s = 0.022$).

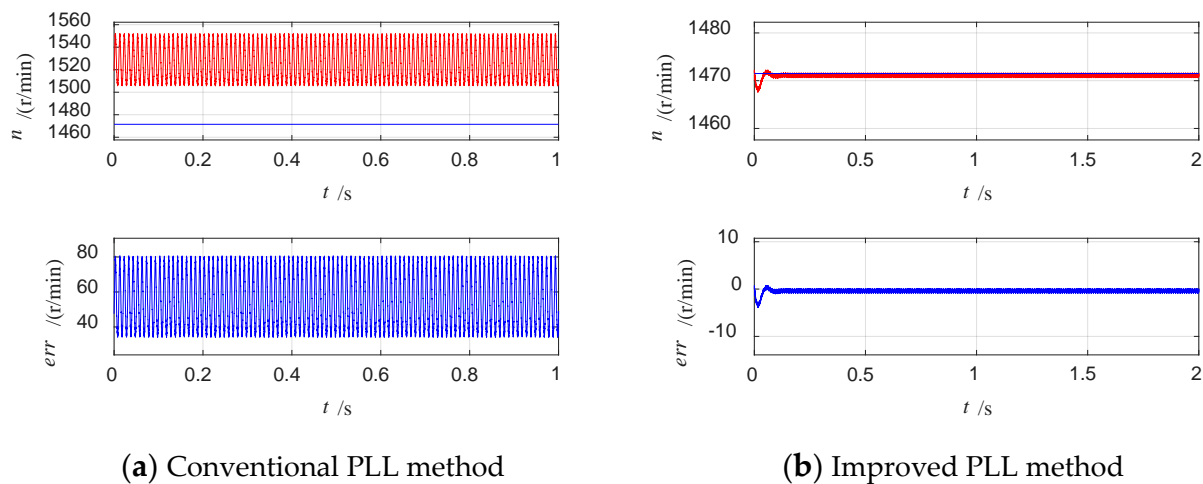


Figure 13. The simulated speed estimation results ($n = 1469$ r/min, $s = 0.019$).

4.3. Online Speed Estimation Results under Different Speed and Load Conditions

Based on the simulation verification, the online speed estimation was further carried out through the established platform shown in Figure 7. The performance comparisons of the conventional and improved PLL methods, along with the original measured phase current and its frequency analysis results, are given under different working conditions of speed 239–1396 rpm and slip ratios ranging from 0.02 to 0.04, respectively, shown in Figures 14–19. It is obvious that the improved PLL method with harmonic separation performed much better in terms of estimation accuracy. In more detail, if the PLL was directly used to process the PSH signal, significant estimation errors appeared in the estimation results, including not only high-frequency dynamic errors but also unacceptable static errors. Static errors made the estimated speed much smaller than the actual one, and the error became more severe as the speed decreased, which indicates that the PLL actually failed to track the value of the PSH signal in real time. Furthermore, the unideal properties of the filters, other motor harmonics, and sensor noises are the main reasons for the increased fluctuation in experimental results compared with simulated ones.

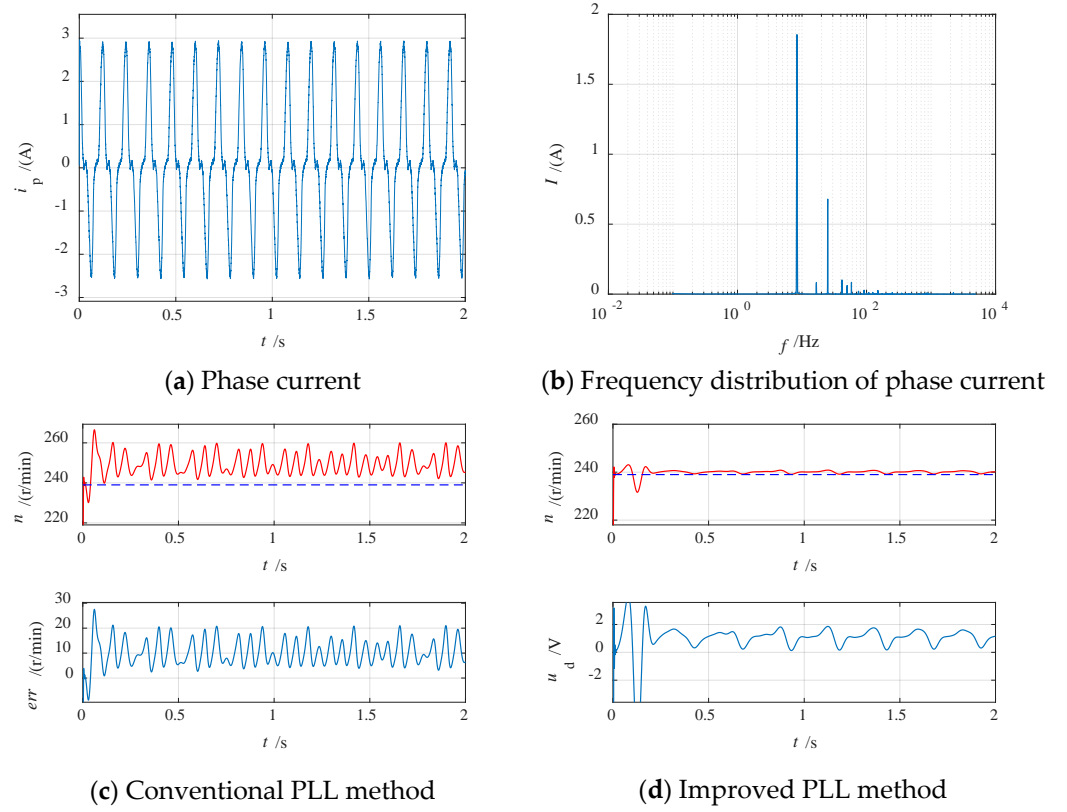


Figure 14. The experimental speed estimation results ($n = 240$ r/min, $s_m = 0.044$, the blue dotted line: the actual value, the red line: the estimated value, same for Figures 15–19).

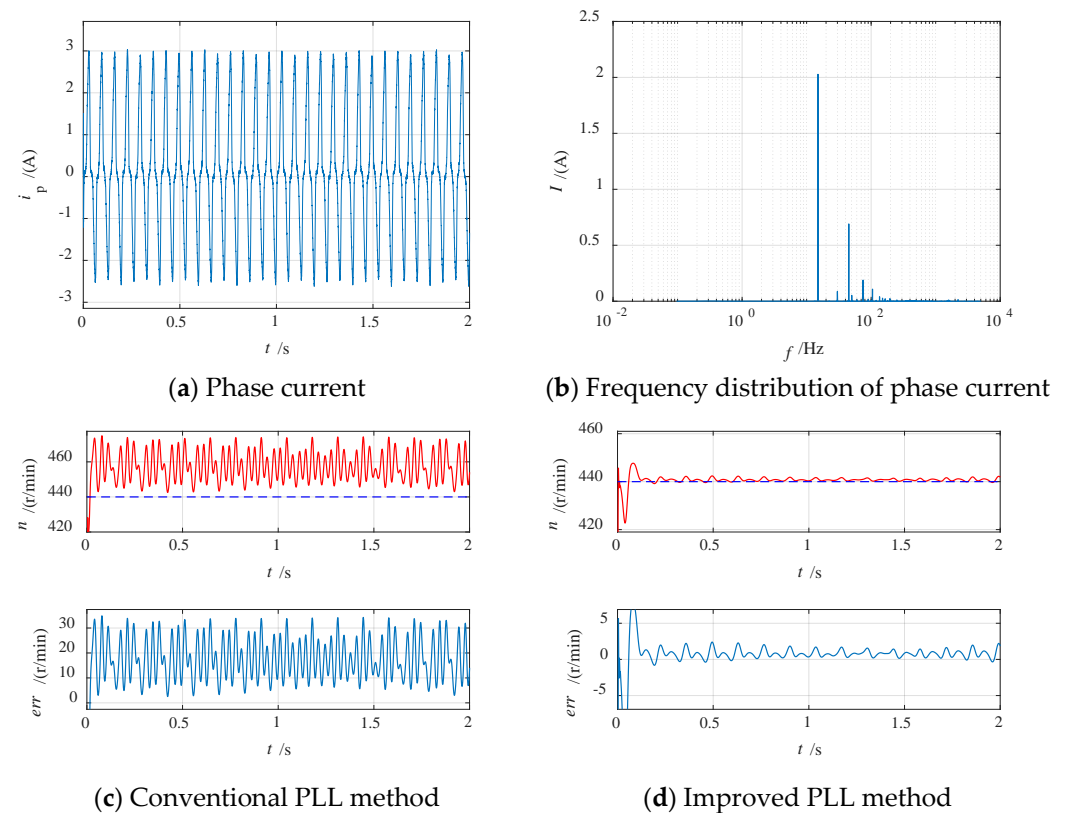


Figure 15. The experimental speed estimation results ($n = 450$ r/min, $s_m = 0.022$ blue dotted line: the actual value, red line: the estimated value).

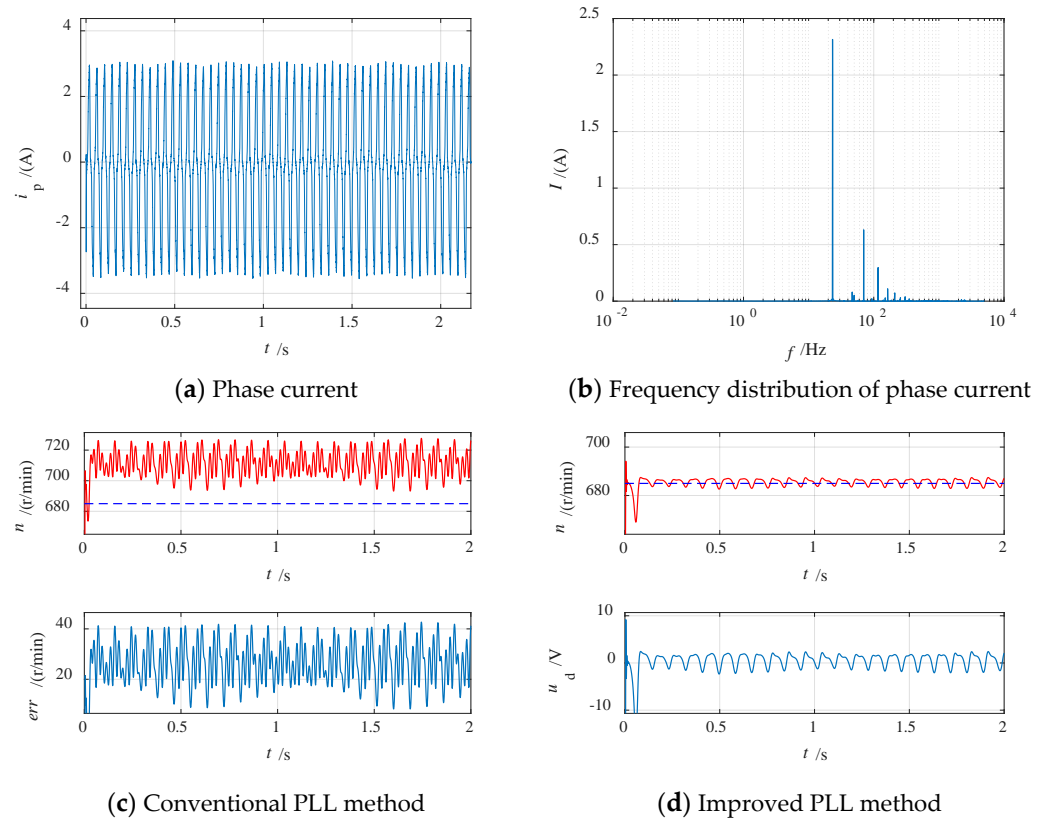


Figure 16. The experimental speed estimation results ($n = 685$ r/min, $s_m = 0.022$).

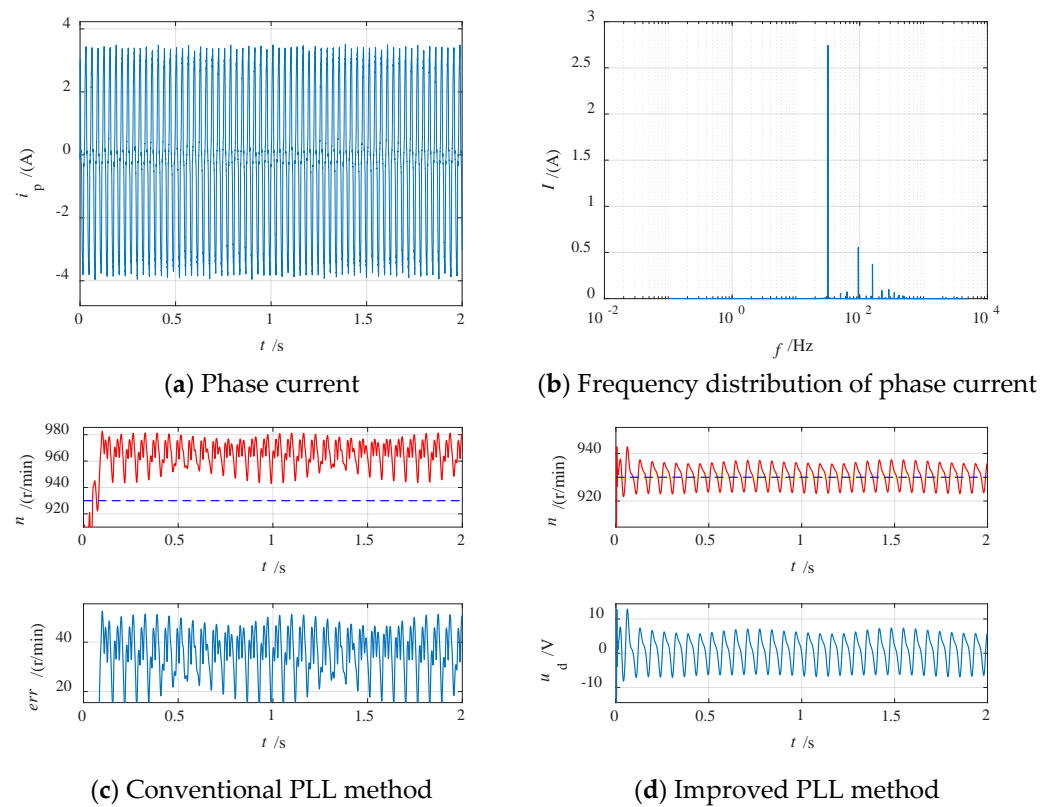


Figure 17. The experimental speed estimation results ($n = 930$ r/min, $s_m = 0.021$).

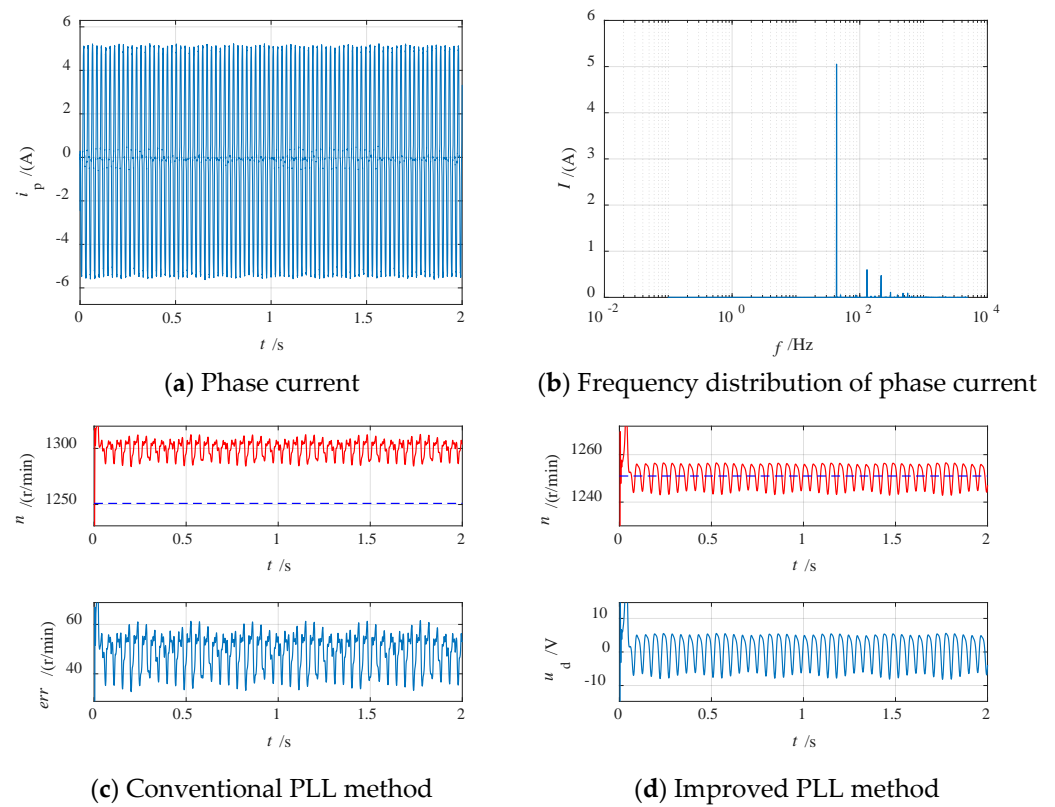


Figure 18. The experimental speed estimation results ($n = 1251$ r/min, $s_m = 0.038$).

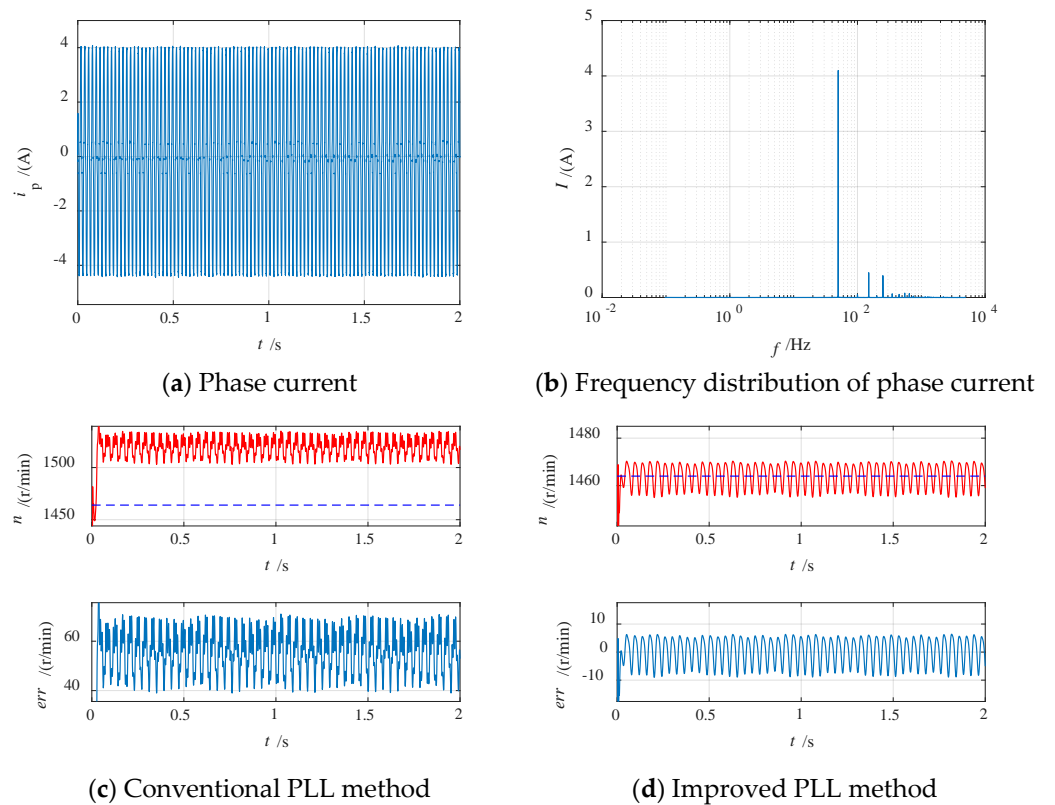


Figure 19. The experimental speed estimation results ($n = 1464$ r/min, $s_m = 0.024$).

As for the estimation results of the improved PLL method, as shown in Figures 14d, 15d and 16d, etc., the PLL performed well due to the steady signal amplitude after the

harmonic separation process. There were more dynamic errors in the experiment compared with the simulation results, which were mainly caused by unfiltered harmonics and noise, but the steady error could always be kept within ± 10 r/min in a wide speed range. More high-frequency dynamic errors could be detected when the motor speed exceeded 900 r/min, as shown in Figures 17d, 18d and 19d. This is because of the included harmonics close to the PSH components as the passband width at high speed became larger, as mentioned in Section 3.

The speed estimation accuracy of the conventional PLL method and the proposed method are listed in Table 2, with both the absolute and relative error calculated. It is obvious that the proposed method performed much better with a relative error smaller than 1%.

Table 2. The estimation error of the conventional PLL method and the proposed method.

Speed n (r/min)	Slip Ratio s_m	Steady Error of the Conventional Method (r/min)	Steady Error of the Proposed Method (r/min)
240	0.044	19.8 (8.25%)	1.8 (0.75%)
450	0.022	32.3 (7.18%)	2.2 (0.49%)
685	0.022	40.9 (5.97%)	2.0 (0.29%)
930	0.021	51.2 (5.51%)	5.9 (0.63%)
1251	0.038	60.5 (4.84%)	7.4 (0.59%)
1464	0.024	69.1 (4.72%)	8.1 (0.55%)

5. Conclusions

In this paper, an improved PLL-based speed estimation method embedded with the harmonic separation method was proposed to cope with properties such as amplitude fluctuation and side-frequency components in the time domain and frequency domain, respectively. Through simulations and experiments, it was proved that the proposed method can effectively estimate the speed of IMs online in a wide speed range, with satisfying accuracy and convergence time.

Since rotor slot harmonics are universal in most induction motors as the rotor is generally slotted regardless of the phase number, the proposed method can be utilized in both the usual three-phase motors as well as specific multiphase motors. The introduced harmonic separation processing helps improve the performance of speed estimation. A remaining problem of the proposed method is that the passbands of the filters for harmonic separation become very narrow in a low-speed range. Meanwhile, in the actual case, besides the PSH and noises, the harmonics are also included in the speed estimation, thus causing high-frequency dynamic errors. These problems still need to be solved in our future works.

Author Contributions: Conceptualization, J.Y. and X.Z.; methodology, Y.Z.; software, Y.Z.; validation, J.Y. and Y.Z.; writing—original draft preparation, J.Y.; writing—review and editing, J.Y.; funding acquisition, J.Y. All authors have read and agreed to the published version of the manuscript.

Funding: This study received funding from the Natural Science Foundation of Shandong Province (Grant No. ZR2021QE118), the Key Project of Innovative Teaching Laboratory of Qingdao University in 2020 (Grant No. CXSYZD202001), and the National College Students Innovation and Entrepreneurship Training Program of China (Grant No. S202011065023).

Institutional Review Board Statement: Not applicable.

Informed Consent Statement: Not applicable.

Data Availability Statement: The data used in this study are available from the authors upon reasonable request.

Conflicts of Interest: The authors declare no conflict of interest.

References

1. Levi, E. Multiphase Electric Machines for Variable-Speed Applications. *IEEE Trans. Ind. Electron.* **2008**, *55*, 1893–1909. [[CrossRef](#)]
2. Diarra, M.N.; Yao, Y.; Li, Z.; Niasse, M.; Li, Y.; Zhao, H. In-Situ Efficiency Estimation of Induction Motors Based on Quantum Particle Swarm Optimization-Trust Region Algorithm (QPSO-TRA). *Energies* **2022**, *15*, 4905. [[CrossRef](#)]
3. Wang, H.; Yang, Y.; Ge, X.; Zuo, Y.; Yue, Y.; Li, S. PLL- and FLL-Based Speed Estimation Schemes for Speed-Sensorless Control of Induction Motor Drives: Review and New Attempts. *IEEE Trans. Power Electron.* **2022**, *37*, 3334–3356. [[CrossRef](#)]
4. Gu, C.; Wang, X.; Shi, X.; Deng, Z. A PLL-Based Novel Commutation Correction Strategy for a High-Speed Brushless DC Motor Sensorless Drive System. *IEEE Trans. Ind. Electron.* **2018**, *65*, 3752–3762. [[CrossRef](#)]
5. Shen, J.X.; Iwasaki, S. Sensorless control of ultrahigh-speed PM brushless motor using PLL and third harmonic back EMF. *IEEE Trans. Ind. Electron.* **2006**, *53*, 421–428. [[CrossRef](#)]
6. Song, X.; Han, B.; Zheng, S.; Chen, S. A Novel Sensorless Rotor Position Detection Method for High-Speed Surface PM Motors in a Wide Speed Range. *IEEE Trans. Power Electron.* **2018**, *33*, 7083–7093. [[CrossRef](#)]
7. Orfanoudakis, G.I.; Sharkh, S.M.; Yuratic, M.A. Combined Positive-Sequence Flux Estimation and Current Balancing for Sensorless Motor Control Under Imbalanced Conditions. *IEEE Trans. Ind. Appl.* **2021**, *57*, 5099–5107. [[CrossRef](#)]
8. Wang, H.; Wu, X.; Zheng, X.; Yuan, X. Virtual Voltage Vector based Model Predictive Control for a Nine-phase Open-end Winding PMSM with a Common DC Bus. *IEEE Trans. Ind. Electron.* **2022**, *69*, 5386–5397. [[CrossRef](#)]
9. Herrejón-Pintor, G.A.; Melgoza-Vázquez, E.; Chávez, J.d.J. A Modified SOGI-PLL with Adjustable Refiltering for Improved Stability and Reduced Response Time. *Energies* **2022**, *15*, 4253. [[CrossRef](#)]
10. Ibarra, L.; Ponce, P.; Ayyanar, R.; Molina, A. A Non-Adaptive Single-Phase PLL Based on Discrete Half-Band Filtering to Suppress Severe Frequency Disturbances. *Energies* **2020**, *13*, 1730. [[CrossRef](#)]
11. Filipović, F.; Petronijević, M.; Mitrović, N.; Banković, B.; Kostić, V. A Novel Repetitive Control Enhanced Phase-Locked Loop for Synchronization of Three-Phase Grid-Connected Converters. *Energies* **2020**, *13*, 135. [[CrossRef](#)]
12. Yang, D.; Yin, L.; Xu, S.; Wu, N. Power Voltage Control for Single-Phase Cascaded H-Bridge Multilevel Converters under Unbalanced Loads. *Energies* **2018**, *11*, 2435. [[CrossRef](#)]
13. Novak, Z.; Novak, M. Adaptive PLL-Based Sensorless Control for Improved Dynamics of High-Speed PMSM. *IEEE Trans. Power Electron.* **2022**, *37*, 10154–10165. [[CrossRef](#)]
14. Gao, Z.; Turner, L.; Colby, R.S.; Leprettre, B. A Frequency Demodulation Approach to Induction Motor Speed Detection. *IEEE Trans. Ind. Appl.* **2011**, *47*, 1632–1642. [[CrossRef](#)]
15. Keysan, O.; Ertan, H.B. Real-Time Speed and Position Estimation Using Rotor Slot Harmonics. *IEEE Trans. Ind. Inform.* **2013**, *9*, 899–908. [[CrossRef](#)]
16. Yu, J.; Shen, H.; Wang, H.; Wu, X. Speed Estimation of Multiphase Induction Motor using Rotor Slot Harmonics with Limited SNR and Dynamic Load Conditions. *IEEE Trans. Ind. Electron.* **2022**. [[CrossRef](#)]
17. Liu, G.; Zhang, H.; Song, X. Position-Estimation Deviation-Suppression Technology of PMSM Combining Phase Self-Compensation SMO and Feed-Forward PLL. *IEEE J. Emerg. Sel. Top. Power Electron.* **2021**, *9*, 335–344. [[CrossRef](#)]
18. Prakash, S.; Singh, J.K.; Behera, R.K.; Mondal, A. A Type-3 Modified SOGI-PLL With Grid Disturbance Rejection Capability for Single-Phase Grid-Tied Converters. *IEEE Trans. Ind. Appl.* **2021**, *57*, 4242–4252. [[CrossRef](#)]
19. Ciobotaru, M.; Teodorescu, R.; Blaabjerg, F. A new single-phase PLL structure based on second order generalized integrator. In Proceedings of the 2006 37th IEEE Power Electronics Specialists Conference, Jeju, Korea, 18–22 June 2006; pp. 1–6. [[CrossRef](#)]